Research Square

Preprints are preliminary reports that have not undergone peer review.
They should not be considered conclusive, used to inform clinical practice,
or referenced by the media as validated information.

Stepwise Cathodic Potential as a Double-Edged Sword for Anammox: Enzyme-Level Inhibition versus Multi-Pathway Compensation in a Biocathode

Liang Qiao
Yancheng Institute of Technology
Wen Xun
Yancheng Institute of Technology
Shifan Shen
Yancheng Institute of Technology
Liangjie Wang
Peking University
Jianye Liu
Originwater Construction Group Co., Ltd
Feihong Wang
Yancheng Institute of Technology
Yan Li
Yancheng Institute of Technology
Luyan Zhang
zly3161@163.com

Yancheng Institute of Technology
Ye Yuan
Yancheng Institute of Technology
Tianming Chen
Yancheng Institute of Technology
Shijun Li
Zhejiang University

Article

Keywords: Anammox, stepwise cathodic potentials, PD/A, multiple nitrogen pathways, potential relay

Posted Date: November 2nd, 2026

DOI: https://doi.org/10.21203/rs.3.rs-11371347/v1

License: This work is licensed under a Creative Commons Attribution 4.0 International License.
Read Full License

Additional Declarations: No competing interests reported.

Stepwise Cathodic Potential as a Double-Edged Sword for Anammox: Enzyme-Level Inhibition versus Multi-Pathway Compensation in a Biocathode

Liang Qiao[a,b], Wen Xun[a], Shifan Shen[a], Liangjie Wang[c], Jianye Liu[d], Feihong Wang[a,b], Yan Li[a,b], Luyan Zhang[a,b,*], Ye Yuan[a,b], Tianming Chen[a,b], Shijun Li[e,*]

a, School of Environmental Science & Engineering, Yancheng Institute of Technology, Yancheng, Jiangsu Province, China

b, Jiangsu Province Engineering Research Center of Intelligent Environmental Protection Equipment, Yancheng Institute of Technology, Yancheng, China

c, The Key Laboratory of Water and Sediment Sciences (Ministry of Education), College of Environmental Sciences and Engineering, Peking University, Beijing, China

d, Originwater Construction Group Co., Ltd, Beijing, China

e, College of Environmental & Resource Sciences, Hangzhou, Zhejiang Province, China

Corresponding author: L. Zhang, School of Environmental Science and Engineering, Yancheng Institute of Technology, Yancheng, 224051, China. E-mail: zly3161@163.com

Corresponding author: S. Li, College of Environmental & Resource Sciences, Zhejiang University, Hangzhou, 310058, China. E-mail: sjli.env@zju.edu.cn

Abstract:

Coupling anammox with bioelectrochemical systems (BESs) offers carbon-free autotrophic nitrogen removal, yet the cathodic potential required for NO_3^- reduction to NO_2^- (+0.433 V vs. SHE) lies far above the activity window of anaerobic ammonium-oxidizing bacteria (AnAOB), creating a fundamental potential gap. Here, anammox biocathodes in dual-chamber BESs were operated under nine stepwise potentials (+0.105 to +0.433 V vs. SHE, with a +0.000 V control), each alternated with +0.433 V in 30-min segments over 3-h cycles, and interrogated through short-term kinetics, 16S rRNA sequencing, and proteomics. Nitrogen removal peaked at +0.145 V (NH_4^+-N 94.1%, NO_2^--N 96.2%), declined to a valley at +0.345 V, and rebounded to 46.7% at +0.385 V as non-anammox pathways compensated for impaired anammox activity. Charge integration of the I–t curves showed that the stepwise cathodic potential acted as a regulatory signal rather than an electron source. The dominant AnAOB genus *Candidatus Brocadia* peaked in abundance (7.96%) at +0.305 V even as activity was suppressed. Nitrification proteins hyperactivated at +0.265 ± 0.04 V alongside excess NO_3^- accumulation, while upregulation of the DNRA protein NrfC implied internal ammonium recycling at high potentials. Hence, a two-stage stepwise-potential-assisted anammox denitrification (SPAD) strategy (+0.145 V × 90 min → +0.385 V × 30 min) was proposed to convert the potential gap into a temporal potential relay for autotrophic nitrogen removal.

Keywords: Anammox; stepwise cathodic potentials; PD/A; multiple nitrogen pathways；potential relay

1 Introduction

1.1 The bottlenecks of anammox and the rationale for electrochemical intervention

Anaerobic ammonium oxidation (anammox) is among the most cost-effective autotrophic biological nitrogen-removal technologies. It directly converts NH_4^+ and NO_2^- to N_2 without external organic carbon, saving approximately 60% of aeration energy, 100% of organic carbon dosage, and 90% of sludge production and reducing N_2O emissions by 35% [1-3]. However, AnAOB have long doubling times and strictly require an NH_4^+/ NO_2^- molar ratio of 1:1.32 [4,5]. In low-C/N wastewaters such as aquaculture effluent, digester supernatant, and landfill leachate after secondary treatment, a stable NO_2^- supply therefore constitutes the core bottleneck for anammox application [6,7].

Two mainstream NO_2^--supply routes have been developed: partial nitritation (PN, $NH_4^+ \rightarrow NO_2^-$) and partial denitrification (PD, $NO_3^- \rightarrow NO_2^-$) [8,9]. PN/A processes chronically suffer from incomplete NOB suppression, comammox interference, and instability in mainstream low-temperature applications [10,11], whereas PD/A requires precise C/N control to avoid over-reduction of NO_2^- to N_2 [12-14]. In low-C/N scenarios, the scarcity of organic electron donors makes stable PD operation difficult, motivating a tunable, carbon-free electron-donor alternative.

BES employs the electrode as a tunable electron donor, providing a new platform for carbon-free denitrification and anammox enhancement in low-C/N wastewaters [15-18]. At a BES cathode, the electrode directly supplies electrons to electroactive microorganisms driving the sequential reductions $NO_3^- \rightarrow NO_2^- \rightarrow NO \rightarrow N_2O \rightarrow N_2$. The electrode potential effectively acts as a regulating valve on the electron flux. Electrochemical routes can thus

provide electron pathways for biological nitrogen removal, opening a carbon-free route to autotrophic denitrification [19,20].

1.2 Advantages and disadvantages of electrochemical intervention in anammox

Electro-assisted PD/A and BES-anammox offer clear advantages. The cathode can drive denitrification and anammox without organic carbon, avoiding the carbon dependence and secondary pollution of heterotrophic PD/A [16,21]. Research have achieved a nitrite-transformation ratio of 60±9% and total nitrogen removal of 90±3% at +0.1 V, with anammox contributing 78±5%, proving the feasibility of autotrophic electrochemical PD/A [21]. Electrode potentials can be adjusted in real time by potentiostat, enabling precise start/stop of $NO_3^- \rightarrow NO_2^-$ reduction and avoiding the over-reduction caused by C/N fluctuations in heterotrophic PD [22,23]. Extracellular electron transfer (EET) can extend the metabolic boundary of AnAOB. Studies have demonstrated that highly enriched *Ca. Kuenenia* and *Ca. Brocadia* communities can oxidize $NH_4^+ \rightarrow N_2$ with the electrode as the sole electron acceptor—no NO_2^- required—with maximum current density at +0.6 V vs. SHE, redefining the electron-acceptor boundary of the anammox reaction [24, 25]. In addition, cathodic NO_3^- reduction consumes H^+, enabling self-alkalinization that suppresses free nitrous acid (FNA), while the cathodic biofilm forms an anaerobic microenvironment favoring AnAOB growth [26,27].

The disadvantages are equally significant. First, the potential gap: the potential required for $NO_3^- \rightarrow NO_2^-$ (at least E=+0.433 V vs. SHE) lies well above the AnAOB optimal window (E=+0.05~0.2 V), and the two cannot be satisfied simultaneously [28,29]. Second, multidimensional inhibition of AnAOB at high potential. E > +0.3 V vs. SHE can tighten

AnAOB cell membranes and irreversibly oxidize intracellular components, damaging anammoxosomal membrane structure and HZS/HDH enzyme activity [29,30]. High potentials also favor the competing hydrogen evolution reaction, lowering coulombic efficiency [31]. Third, nitrification side reactions. The enrichment of AOB such as *Nitrosomonas* at high potential, with significant upregulation of AmoABC/Hao proteins, diverts part of the NH_4^+ to NO_2^-/ NO_3^- and adds redundant nitrogen cycling [32,33]. And the decline of nosZ-containing taxa such as *Ignavibacterium* at high potential may cause transient N_2O accumulation [34,35]. Moreover, continuous energization may cause electrode polarization, charge accumulation, and biofilm detachment, making sustained anammox activity difficult and compromising long-term stability [29,36].

1.3 The double-edged-sword problem of stepwise potential on Anammox

As the energy switch of cathodic metabolism, potential affects AnAOB activity in a strongly potential-dependent and bidirectional manner, spanning a low-potential stimulation window (E=+0.05~+0.2 V vs. SHE) and a high-potential inhibition threshold (E ≥ +0.3 V vs. SHE). Yin et al. found in a three-electrode MEC that E=+0.05~+0.2 V enhanced anammox activity by 25%, with cyclic voltammetry identifying a redox couple at +0.08 V vs. Ag/AgCl associated with c-type cytochromes [28]. Cai et al. applied E=−0.36 V vs. SHE weak stimulation in a two-chamber BES, raising nitrogen removal by 60.6% with electron-transport-system activity of 34.2 μg/(mg·h) [29]. Hu et al. reported a 140% NRR enhancement (11.2 g N/(m^2·d)) at E=−0.7 V vs. Ag/AgCl in a marine anammox system, with *Ca. Brocadia* enriched to 7.5% on the cathode [30]. Priks et al. achieved 100% TN removal within 150 h at E=−0.7 V vs. Ag/AgCl [37]. Tang et al. found that high anode potentials

(0.3~0.4 V vs. SHE) promote DNRA while suppressing NOB [38].

Existing studies have focused almost exclusively on long-term acclimation under single, steady potentials [28-30,37], whereas the acute kinetic response to stepwise potential, the transient reconfiguration of nitrogen-transformation pathways, and the rapid microbial–enzymatic feedback remain poorly understood. In particular, stepwise operation must reconcile the positive effects of potential with its negative effects. Thus, a control strategy that simultaneously protects anammox activity and secures substrate supply is essential.

1.4 Principal nitrogen-transformation pathways under stepwise potentials

Nitrogen conversion at the biocathode is not a single anammox route but a cooperative network of parallel pathways. (a) Anammox pathway is the dominant route at low potentials [24,39]. Wang et al. recently reported that ferroheme/ferriheme directly participates in N_2H_4 synthesis and decomposition as an electron carrier; Zheng et al. further showed that siderophore-mediated cooperation among AnAOB enhances anammox activity [40,41]. (b) Heterotrophic/autotrophic denitrification pathway. In BES cathodes the electrode serves as direct electron donor for autotrophic denitrification, with *Denitratisoma*, *Thauera*, and *Comamonas* as common dominant genera [21,29]. (c) Nitrification pathway. At high potential, enrichment of AOB such as *Nitrosomonas* significantly activates nitrification side reactions, a key mechanism underlying anomalous NO_3^- accumulation. (d) DNRA pathway. Wang and Qiao revealed the electron-transfer mechanism of endogenous DNRA inside anammox bacteria, achieving >95% TN removal by AnAOB alone and breaking the theoretical 89% TN-removal ceiling of anammox [42]. Dong et al. confirmed DNRA–anammox synergy reaching 100% NH_4^+ removal and 94.25% TN removal in a g-C_3N_4–

anammox system [43]. Guo et al. further demonstrated NO_3^- removal by AnAOB utilizing photoexcited electrons via an inward EET channel [44]. (e) Assimilatory nitrate reduction for biosynthesis, and (f) nitrogen fixation [45,46].

1.5 Objectives of this study

Against the backdrop of this double-edged-sword problem and the multi-pathway network, we investigated the acute response mechanism of an anammox biocathode under stepwise potentials. The specific objectives were: (a) to identify the acute tolerance threshold and optimal operating window of the anammox biocathode under stepwise potentials; (b) to resolve how potential transitions reshape cathodic biofilm community structure and nitrogen-transformation pathways, and to quantify the contribution and synergy of non-anammox pathways at high potential; (c) to reveal the differentiated expression of anammox-related and denitrification-related functional proteins across potentials at the protein level.

2 Methods and Materials

2.1 Reactor configuration and anammox biocathode setup

Four identical dual-chamber bio-electrochemical reactors were constructed (R1–R3 and a CE control). Each reactor consisted of two 28 mL rectangular acrylic chambers joined together with total volume 56 mL, separated by a proton-exchange membrane (Nafion 117, DuPont) (Fig. 1). Anode and cathode were connected through an electrochemical workstation (CHI1000C, Chenhua, Shanghai). The cathode potential was controlled against a saturated calomel electrode (SCE, +0.241 V vs. SHE). A carbon brush (φ30 mm × 5 mm) served as the anode, and the anodic chamber was filled with 28 mL of 1 mol/L $K_4[Fe(CN)_6]$.

The cathode was a U-shaped carbon brush pretreated by ethanol impregnation (48 h) →

thermal activation under inert atmosphere (600 °C, 30 min) → deionized-water rinsing → pre-soaking in anammox synthetic medium for 2 h. Each reactor was inoculated with 20 mL of anammox granular sludge from a laboratory upflow reactor operated at 30 ℃ for 18 months. The SCE reference electrode and granular sludge were placed inside the U-shaped cathodic chamber to ensure close contact.

The synthetic wastewater contained NH_4^+-N 85.52 ± 12.04 mg/L (NH_4Cl), NO_2^--N 94.90 ± 2.37 mg/L ($NaNO_2$), and $KHCO_3$ 2 g/L, with an NH_4^+/ NO_2^- molar ratio of 1:1.11 (slightly below the theoretical 1:1.32 to ensure the culture was not NO_2^--limited). Reactors were maintained in a 33.0 ± 0.5 °C water bath.

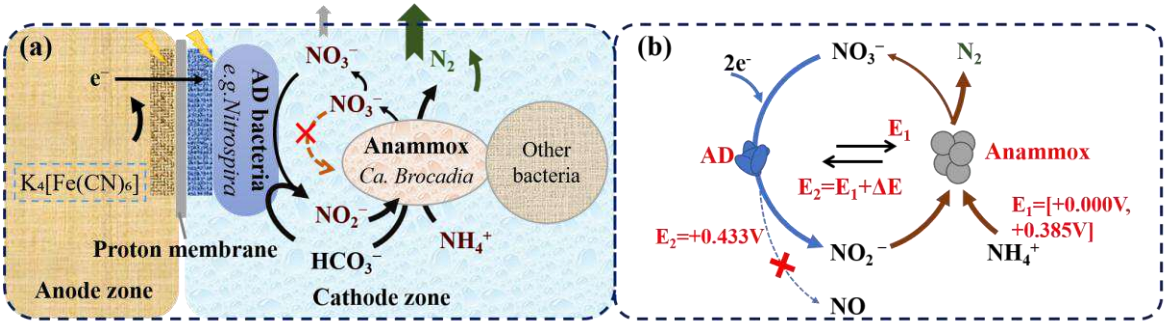


Fig. 1 Main nitrogen transformation pathways of the cathode. (a) schematic of the reactions; (b) reaction at the cathode surface and attached microorganisms at selected potentials

2.2 Potential-step experiments and short-term kinetic monitoring

Cathodic potentials were set at nine values spanning +0.000 V to +0.433 V vs. SHE (+0.105, +0.145, +0.185, +0.225, +0.265, +0.305, +0.345, +0.385, +0.433 V), covering the biological stimulation window of AnAOB (E=+0.105~E=+0.225 V), the critical potential for direct NO_2^- reduction at the electrode surface (E=+0.385 V), and the thermodynamic threshold for NO_3^-→NO_2^- (E=+0.433 V) [16,19, 28-30]. Each 3-h cycle consisted of six consecutive 30-min segments, in which the designated potential and E=+0.433 V (vs. SHE) were alternately applied (designated potential: 0–30, 60–90, and 120–150 min; E=+0.433 V:

30–60, 90–120, and 150–180 min). The CE group was held at E=+0.000 V vs. SHE. After the potential was applied, the cathode potential was adjusted to E=+0.05 V, and it was adjusted to the potential of the next stage after 2 days of operation. Every 24 h the cathodic chamber was completely replenished with 28 mL fresh synthetic medium (withdrawn in two steps: 28 mL removed, 5 min settling, residual removed, then 28 mL added). Each stepwise-potential batch ran 3 h with 1.5 mL samples taken at t = 0, 0.5, 1.0, 1.5, 2.0, 2.5, 3.0 h (filtered through 0.22-μm membranes, stored at 4 ℃). At the end of selected batches, 1.5 mL of sludge was collected near the cathodic biofilm, flash-frozen in liquid nitrogen, and stored at −80 ℃ for microbial-community and proteomic analysis. NH_4^+-N, NO_2^--N, and NO_3^--N were determined by the nesslerization (GB 7479-87), N-(1-naphthyl)-ethylenediamine (GB 7493-87), and dual-wavelength UV (HJ/T 346-2007, 220/275 nm) methods, respectively. Current was recorded at 4.0-s intervals for electron-flux calculations.

2.3 Nitrogen-balance calculation

Nitrogen balances were based on the canonical anammox stoichiometry NH_4^+: NO_2^-: NO_3^- = 1:1.32:0.26 [4]. Because each stepwise batch lasted only 3 h, net biomass growth and assimilation were negligible. Substrate degradation rates ($\Delta c/\Delta t$) were obtained by linear regression of concentration–time curves (mg N/(L·h)), and biomass-specific rates were calculated with the inoculated granular-sludge VSS (VSS = 0.129 g/mL). The electrochemical contribution to nitrogen conversion was quantified from the integrated charge $Q = \int I\,dt$ over the 3-h potential application. Under the stepwise operation mode, Q was integrated for each 30-min segment, and $n(e^-)$ and m(N) were calculated as:

$$n(e^-)=Q/F$$

$$m(N)=n(e^-)/v\times A_r$$

where A_r = 14 g/mol is the atomic mass of nitrogen, F= 96485 C/mol, and ν = 2 for $NO_3^- \rightarrow NO_2^-$.

Key cathodic half-reactions (25 °C, pH 7, vs. SHE):

$$NO_2^- + 2H^+ + e^- \rightarrow NO + H_2O \ (E= +0.350\ V)$$

$$NO_3^- + 2H^+ + 2e^- \rightarrow NO_2^- + H_2O \ (E= +0.433\ V)$$

Given the applied potentials, multiple nitrogen-conversion routes exist are feasible. Because E=+0.433 V is far below the potential required for $NO_2^- \rightarrow N_2$ (E= +1.355 V), electrochemical nitrogen conversion in this system is confined to $NO_3^- \rightarrow NO_2^-$; subsequent NO_2^- reduction to N_2 proceeds through biological pathways (anammox or denitrification).

2.4 Microbial community and metabolic pathway analysis

High-throughput sequencing characterized taxonomic shifts in the cathode-associated biofilms before and after potential application. Proteomic analysis quantified expression changes of key functional proteins, specifically targeting anammox enzymes (hydrazine synthase, hydrazine dehydrogenase), nitrogen-cycling machinery (NarG, NapA, NirS/K, NrfA, etc.), and electron-transfer components (c-type cytochromes, flavoproteins). All sequencing and proteomic analyses were conducted by Shanghai Biozeron Biotechnology Co., Ltd. under standardized quality-control protocols (Supplementary Materials, 1 Proteomic analysis).

3 Results and Discussions

3.1 Dynamics of the three nitrogen species and the optimal potential window

Under the stepwise potentials, the 3-h evolution of NH_4^+-N, NO_2^--N, and NO_3^--N in the

cathodic chamber displayed a clear low-potential promotion, high-potential inhibition pattern (Fig. 2).

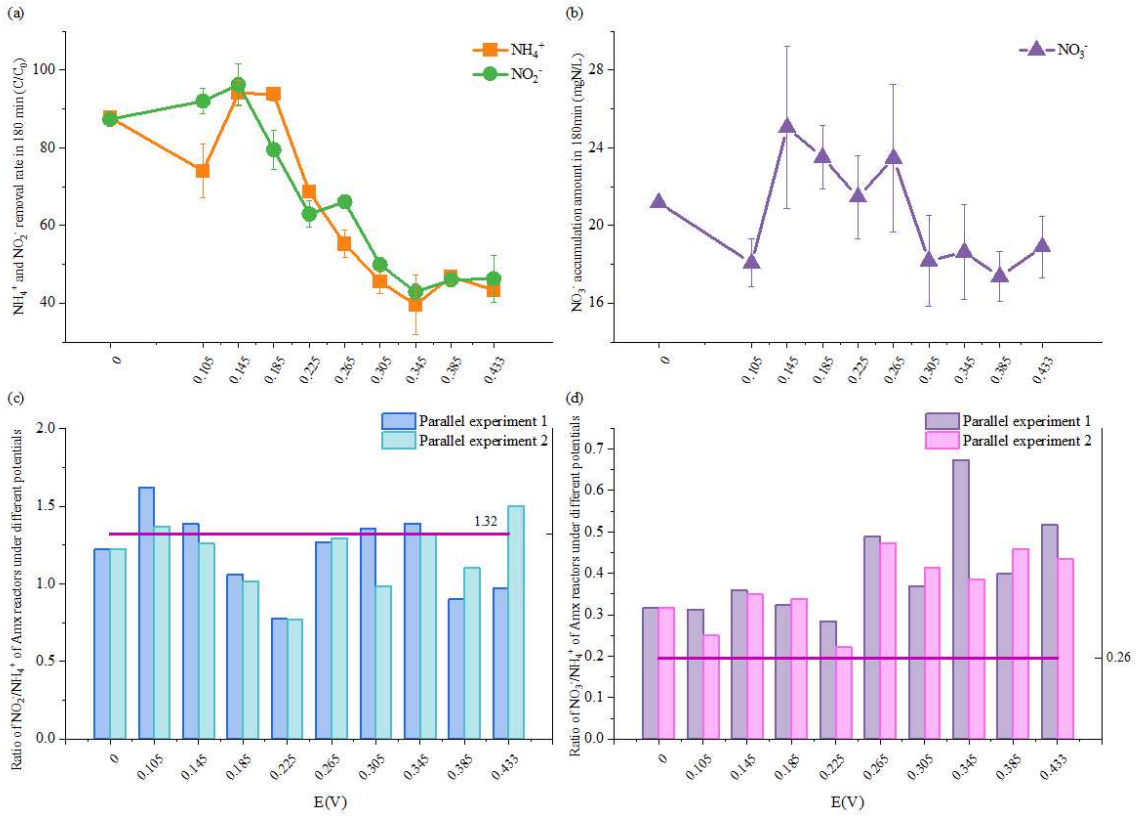


Fig. 2. NH_4^+ and NO_2^- converted in 180 min under different potentials, and NO_3^- generated (C/C_0). (a) conversion rates of ammonia nitrogen and NO_2^-; (b) amount of NO_3^- generated; (c) NO_2^-/NH_4^+ ratio for each parallel test; (d) NO_3^-/NH_4^+ ratio for each parallel test

According to the potential effect and substrate removal efficiency, the potentials fall into three zones. Stage 1 (E = +0.105~0.185 V, enhanced-anammox zone). NH_4^+ removal over 3 h was 74.1 ± 0.7%, 94.1 ± 3.1%, and 93.8 ± 1.0%, with NO_2^- removal of 92.0 ± 2.5%, 96.2 ± 2.6%, and 79.5 ± 0.8%. E=+0.145 V was the optimal potential, with removal clearly exceeding the open-circuit control (NH_4^+ 87.8%, NO_2^- 87.3%); NO_3^- production was peaked at +0.145V (25.06 ± 0.82 mg N/L), coinciding with maximal substrate removal at +0.145 V and consistent with stoichiometric anammox plus minor nitrification, with the NO_3^--produced/ NH_4^+-consumed ratio slightly above 0.26. In addition, NH_4^+ removal at +0.105 V (74.1%) and NO_2^- removal at +0.185 V (79.5%) fell below the CE control, whereas +0.145

V exceeded the control on both substrates. Within this range, anammox dominated with negligible nitrification and denitrification. Stage 2 (E = +0.225~0.345 V, gradient-inhibition zone). NH_4^+ removal declined stepwise through 68.5 ± 2.1%, 55.3 ± 2.9%, and 45.4 ± 2.5%, indicating moderate inhibition of anammox activity. NH_4^+ and NO_2^- removal dropped to 39.4 ± 1.7% and 42.7 ± 4.9%, the minimum of the series at E=+0.345 V. Stage 3 (E = +0.385~0.433 V, V-shaped rebound). Removal rebounded to 46.7 ± 2.3% (NH_4^+) and 46.0 ± 0.6% (NO_2^-) at +0.385 V. This V-shaped profile is consistent with the low-potential promotion—high-potential inhibition pattern observed by Hu et al. [30] in an anammox-MEC, and is presumably driven by the onset of electrochemical NO_3^-→NO_2^- reduction at high potential, which partially compensates the direct inhibition of AnAOB by supplying additional NO_2^- [16,21,25]. The $\Delta NO_3^-/\Delta NH_4^+$ ratios exceeded 0.26 at all potentials (with +0.225 V, at 0.28, closest to the theoretical value), indicating additional NO_3^--generating pathways in the reactor.

To capture the kinetic features of the stepwise response, substrate degradation rates were regressed separately over 0–90 min and 90–180 min (Fig. 3). The maximum NH_4^+ rate in the 0–90 min window occurred at E=+0.145 V (27.52 mg N/(g VSS·d)), 2.2-fold that of the same potential in 90–180 min. The NO_2^- rate at E=+0.145 V was 32.29 mg N/(g VSS·d), exceeding the 90–180 min value of the same potential by 2.1~3.0-fold (Fig. 3 (a) and (c)). NO_3^- net-accumulation rates in the 0–90 and 90–180 min windows were similar within E=+0.105~0.185 V, and above E=+0.265 V, accumulation accelerated anomalously, far exceeding the theoretical anammox contribution, indicating extra NO_2^-→NO_3^- pathways exceeded (NO_2^- oxidation or nitrification) (Fig. 3(e)). Compared with the CE group, NH_4^+

and NO_2^- rates at E=+0.105~0.185 V were close to control values, while all higher potentials fell below the control. Inhibition was significant beyond E=+0.305 V, with rates reduced by >50% at some potentials. This is consistent with the enhanced AnAOB metabolism observed under −0.36 V weak cathodic stimulation [29]. The first 90 min after a potential step thus represents the most vigorous microbial response, after which substrate depletion and prolonged high-potential exposure allow inhibition to dominate. Therefore, two parallel mechanisms were inferred: (i) at E ≥ +0.385 V electrons flowed directly to NO_2^- reduction, generating NO and N_2O and lowering the effective NO_2^- availability to anammox [21]; and (ii) E> +0.3 V caused intracellular oxidation that may damage the anammoxosomal membrane and HZS/HDH activity [29,30]. Furthermore, the temporal variation in the difference between the reaction rates of NH_4^+ and NO_2^- at the same applied potential during the periods of 0–90 min and 90–180 min, along with the significant attenuation of the reaction rate at higher potentials, indicated that low potential enhanced the anammox process. As the potential increased, the reaction rate of NH_4^+ decreased, whereas that of NO_2^- increased. Notably, at high potentials beyond 90 min, the reaction rate of NO_2^- within the system increased, accompanied by internal surface side reactions involving NO_2^-. In contrast, the formation rate of NO_3^- remained relatively low under low-potential conditions with the absolute yield peak of NO_3^- at E=+0.145 V, suggesting that anammox was the primary pathway for nitrogen conversion at this stage. The reduction in NO_3^- production observed in the potential range of E=+0.225~0.305 V was primarily attributed to a series of side reactions involving low-valence nitrogen species. When the applied potential exceeded E=+0.345 V, the accumulation of NO_3^- in the system increased, indicating the presence of a conversion

pathway from NO_2^- to NO_3^- (Fig. 3(b), (d), (f)).

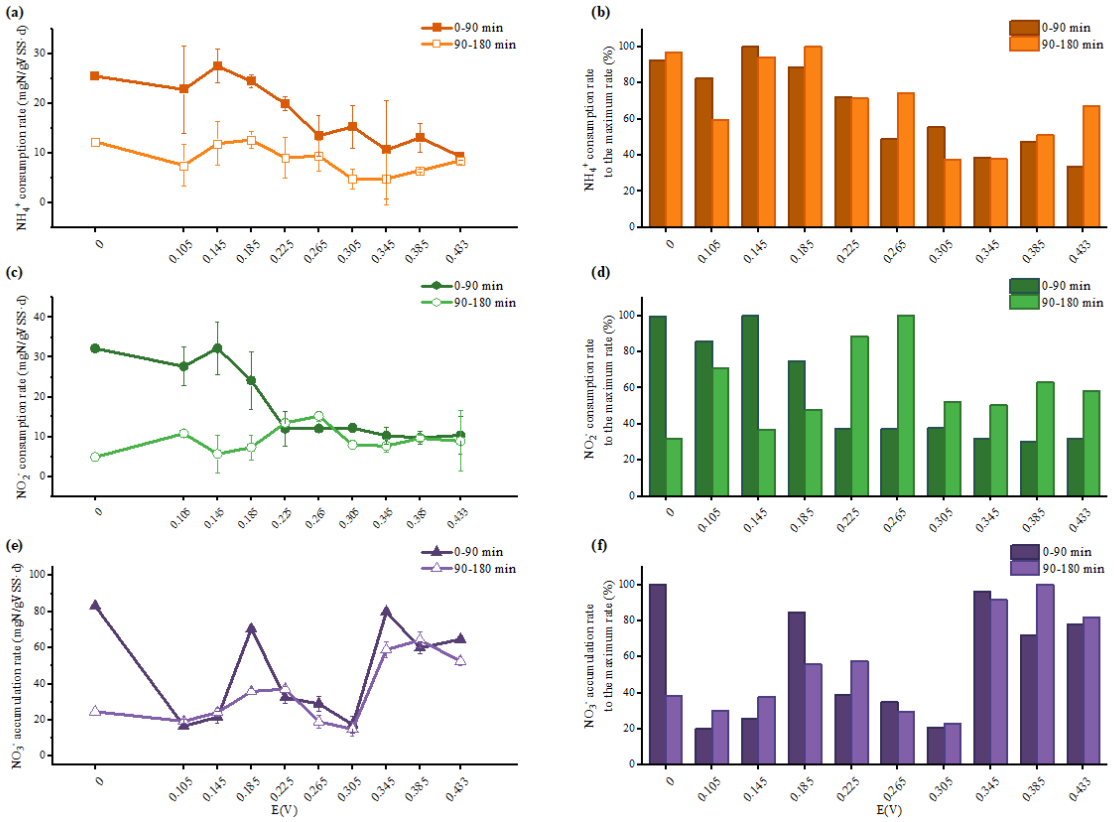


Fig. 3 Specific reaction rates of each potential and the ratios of the specific rates to the maximum rate over 0-90min and 90-180min

The deviation of measured NO_3^- from the anammox theoretical value was examined to verify the nitrification side reaction. In the CE group the deviation was 9.66 mg N/L. Over E=+0.105~0.185 V the measured NO_3^- exceeded the theoretical value by 4.76±1.72 mg N/L, broadly consistent with anammox dominance. Over E=+0.225~0.305V the excess grew markedly (e.g., +0.265V: measured 23.46 mg N/L vs theoretical 12.46 mg N/L, an excess of 11.00 mg N/L), indicating an additional NO_2^-→NO_3^- oxidation route. Over E=+0.345~0.433V measured NO_3^- remained above theory, with the largest deviation at E=+0.345V. At E=+0.433V the deviation narrowed slightly relative to E=+0.345V, suggesting that NO_3^-→NO_2^- reduction partially offset the accumulation. This NO_3^- accumulation was further interpreted through microbial abundance data below.

To quantify the direct electrochemical contribution, the cumulative charge transferred at the working electrode was integrated from the recorded I–t curves for each 30-min segment (Tab. 1). Within each 3-h cycle, the transferred charge ranged from 1.8 to 58.5 mC across the potential series, with the highest values recorded at E=+0.145 and E=+0.185 V. Even if all of this charge had driven nitrate-to-nitrite reduction, the electrochemical nitrogen conversion would amount to ≤ 4.2 μg N per cycle — 0.2% of the total nitrogen converted. Thus, direct electrochemical electron transfer contributed negligibly to nitrogen transformation. The stepwise cathodic potential acted as a regulatory signal that reconfigured the nitrogen-transforming community and proteome, rather than as a significant electron source.

Tab. 1. Electric quantity (Q value) per 30 min under each stepwise potential

Q (mC)	CE	0.105V	0.145V	0.185V	0.225V	0.265V	0.305V	0.345V	0.385V	0.433V
0-30 min	0.013	0.101	2.070	3.540	0.457	0.285	1.610	1.180	0.532	1.580
30-60 min	0.647	0.766	4.480	16.250	0.567	0.391	3.780	0.445	0.525	2.360
60-90 min	0.116	0.192	2.160	4.030	0.474	0.258	0.946	0.362	0.470	1.020
90-120 min	0.504	0.750	4.770	14.940	0.631	0.377	1.880	0.366	0.517	1.490
120-150 min	0.124	0.250	2.110	4.490	0.496	0.253	0.854	0.311	0.459	0.889
150-180 min	0.371	0.747	4.890	15.240	0.405	0.378	1.390	0.280	0.506	1.110
Total amount	1.776	2.807	20.480	58.490	3.030	1.943	10.460	2.944	3.009	8.449

Tab. 2 compares the optimal potential window of this study with the literature. Our window agreed with the E=+0.050~0.200 V stimulation range of Yin et al. and additionally captures the acute response threshold (0–90 vs 90–180 min) under stepwise operation [28]. Compared with the negative-potential gains reported, the positive window identified in this study was easier to implement in engineering practice and avoids hydrogen evolution [30,37].

Tab. 2 Comparison between the optimal potential window of anammox in this study against the literature

References	Reactor configuration	Anammox species	Optimal potential (V vs. SHE)	Promotion of NRR
[28]	Three-electrode MEC	Mixed AnAOB	+0.05~+0.20	25%
[29]	Double chamber	Granular sludge	-0.36	60.6%

	BES			
[30]	Single chamber	Marine Anammox	-0.3~-0.7	140%(-0.7V)
	MEC			
[37]	EANR	*Ca. Brocadia*	-0.7	+140%
[24]	MEC	*Ca. Kuenenia*	+0.6	/
[21]	Double chamber	Mixed sludge	+0.1	60%
	BES			
This study	Double chamber	*Ca. Brocadia*	+0.145	107%*
	BES			

* This was calculated by formula: $P = \text{average}(\Delta\frac{C}{C_0}{}^{E=+0.145V}_{NH_4^+} + \Delta\frac{C}{C_0}{}^{E=+0.185V}_{NH_4^+}) \Big/ \Delta\frac{C}{C_0} CE$

This study indicated that the 0–180 min interval can serve as a local descriptor of the effect of potential on the growth kinetics of anammox bacteria. Our results suggested that under a constant potential of +0.145 V, prolonged electrification combined with timely substrate replenishment can rapidly enhance the removal of both NH_4^+ and NO_2^-. It should be noted that microorganisms in the electrochemical reactor were capable of improving the substrate concentration. The initial substrate concentrations (TN) employed in this study were around 200 mg N/L, which were lower than the substrate tolerance levels of anammox bacteria reported in our previous work [47]. The substrate concentration was not adjusted to such a high level in this study. On one hand, when the substrate concentration was below 50 mg N/L, the specific growth rate of anammox bacteria exceeds that observed at higher substrate concentrations [37]. On the other hand, considering both prior studies and real-world application scenarios—such as the total nitrogen concentrations typically found in domestic wastewater and aquaculture effluent—the NH_4^+ and NO_2^- concentrations used here were substantially higher than those commonly encountered. Therefore, it can be concluded that low applied potential significantly promotes anammox activity. This study did not attempt to further elevate the substrate concentration under low-potential conditions. Nevertheless, it was preliminarily hypothesized that at a potential of E=+0.145 V, the

substrate loading could be further increased, and that the combination of moderately low substrate concentrations with electrical stimulation may synergistically enhance anammox growth.

After completing the E=+0.433 V maximum-potential exposure, the potential of R1-R3 was returned to E=+0.145 V and the reactors were operated for 3 consecutive days: NH_4^+ removal recovered to 89.3 ± 3.2% and NO_2^- to 92.1 ± 2.8%, i.e., 94.9% and 95.7% of the optima. This agreed with the good reversibility of AnAOB at moderate potentials (≤ +0.5 V) [30], indicating that the high-potential inhibition in this short time was primarily transient enzyme-level inhibition rather than cell death or irreversible damage. For engineering practice this implied that occasional potential excursions can be tolerated provided the potential was promptly returned to the safe window with sufficient recovery time (2–3 d). Because this study addressed short-term exposure, whether longer-term repeated exposure–recovery cycles cause cumulative fatigue requires verification.

3.2 Potential-driven succession of the cathodic microbial community

At the phylum level (Fig. 4), *Proteobacteria* was always dominant (38.68%–58.55%, averaging 46.74%), peaking at E=+0.145 V (58.6%). *Planctomycetota* remained stable at 3.13%–4.06%. *Acidobacteriota* was generally more abundant in electrified groups than in the unelectrified raw sludge. *Campylobacterota* was enriched across electrified groups, with markedly elevated abundance at mid-high potentials — E=+0.225 V (15.78%), E=+0.385 V (13.58%) — versus CE (10.88%). Driven by TN loading, these taxa express nitrate reductases (napAB and/or narGH) to reduce nitrate to nitrite and can perform autotrophic denitrification using the electrode as electron donor at high potential. *Bacteroidota* was

significantly higher at E=+0.105 V (8.10%) and E=+0.145 V (9.82%) than after E=+0.185 V (2.03%–3.17%), associated with enrichment of fermentative denitrifiers at low potential [9]. *Nitrospirota* peaked at E=+0.265 V (9.06%) and E=+0.305 V (9.08%), indicating active NOB proliferation at mid potential as the biological basis of the nitrification side reaction, consistent with the anomalous NO_3^- accumulation at these potentials. The high nirK expression of *Nitrospirota* generates NO, while *Planctomycetota* can bind NO, maintaining nitrogen removal under anaerobic conditions — a nitrogen-removal route co-existing in this system. Taken together, these taxa likely participate in NO_3^-→NO_2^- reduction and NH_4^+→NO_2^- oxidation under the applied potentials.

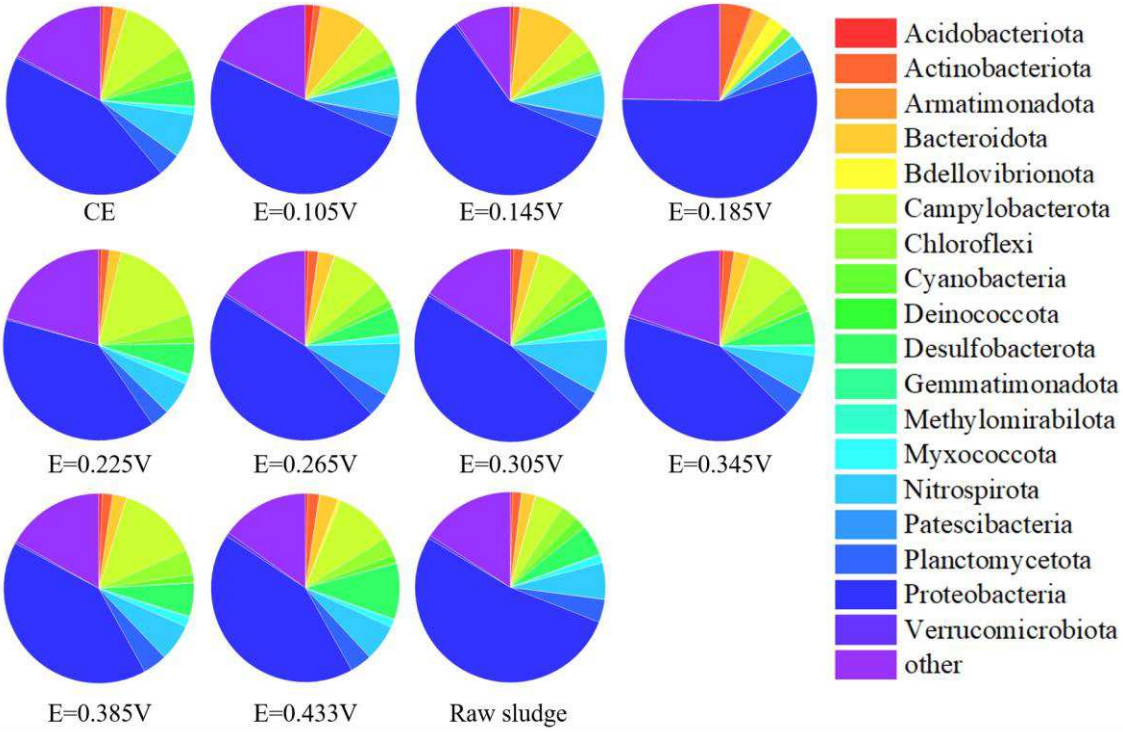


Fig.4 Community composition at the phylum level

At the genus level (Fig. 5), nitrogen-cycling taxa comprised anammox bacteria, facultative anaerobic denitrifiers, and aerobic denitrifiers. Because inter-genus abundance spans orders of magnitude, Fig. 5 displays the relative abundance (R_A) of each genus, calculated as:

R_A=(actual detected abundance)/(1 − Others − Unclassified) × 100%

The absolute abundances are provided in the main text.

The AnAOB genus *Candidatus Brocadia* averaged 6.76 ± 1.30% (excluding the raw sludge and CE), with non-monotonic succession: E=+0.105 V (7.49%) → E=+0.225 V (5.40%) → E=+0.305 V (7.96%, the series maximum among the potential treatments) → E=+0.433 V (3.67%). Minor *Candidatus Jettenia* appeared, consistent with high-potential suppression of AnAOB [28]. Notably, the change in AnAOB abundance (7.49%→3.67%, −51%) is smaller than the change in anammox rate (27.52→11.0 mg N/(g VSS·d), −60%), indicating that abundance loss explains only part of the activity decline — the dominant inhibition is intracellular enzyme damage.

Denitratisoma (10.93%–13.62%) persisted at high abundance across all potentials; its nar, nirS/nirK, and nor genes can participate in the complete NO_3^-→NO_2^-→NO→N_2O denitrification cascade [48], making it the core denitrifier of this low-C/N reactor. *Thauera* was higher at E=+0.433 V (0.14%) than at low potentials (0–0.07%) and may accept electrons at the cathode surface participating in NO_3^- reduction [21,31]. *Comamonas* (facultative aerobic denitrifier) showed two enrichment peaks at E=+0.185 V (0.055%) and E=+0.433 V (0.159%), while the abundance at E=+0.345V and E=+0.385V was approximately 0.105%, indicating bidirectional tolerance to mid–high potentials [49]. *Nitrosomonas* rose from 1.67% at E=+0.145 V to 3.96% at E=+0.225 V when E exceeded +0.185 V, stabilizing at 3.51%–4.50% over E=+0.305~+0.433 V and reaching its maximum (4.50%) at E=+0.433 V. As a chemolithoautotrophic AOB, its anomalous enrichment is consistent with the upregulation of amoABC and Hao in the metaproteome, indicating a

significant nitrification side reaction — the microbiological explanation for the elevated NO_3^- accumulation in this range. Its increase with potential suggests *Nitrosomonas* may accept electrons at the electrode surface for nitrogen conversion. Other functional taxa include *Candidatus Competibacter* (0.025 ± 0.026%), capable only of NO_3^- reduction, and *Ignavibacterium* (declining from E=0.105V 2.41% to E=0.265V 0.19%, slowly increasing to E=0.433V 0.055%), whose decline directly weakens nosZ-mediated $N_2O \rightarrow N_2$ reduction. The role of *Nitrospira* remains unclear: as a NO_2^--oxidizing NOB in a COD-free system, its persistence may rely on trace dissolved oxygen or organic carbon released from cell decay.

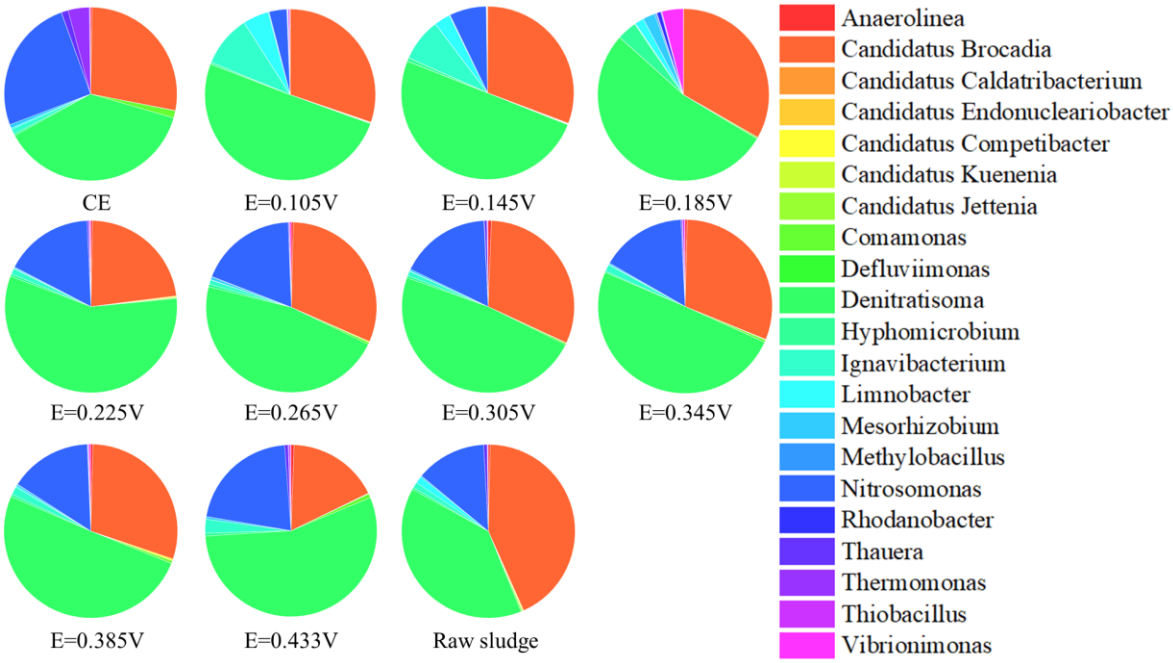


Fig. 5 Community composition at the genus level (relative abundance, RA)

In summary, beyond E=+0.305 V the anammox-dominated community yields to a denitrifier-AOB-sulfur-oxidizer assemblage, and cathodic nitrogen conversion reconfigures from a single anammox route into: the anammox pathway; heterotrophic/autotrophic denitrification (dominated by *Denitratisoma*, *Thauera*, *Comamonas*); nitrification side reactions (*Nitrosomonas* + *Nitrospira*); and DNRA. *Thauera* and *Limnobacter* on the cathode

surface may act as electron shuttles; *Denitratisoma*, *Nitrosomonas*, *Thiobacillus*, and *Rhodocyclaceae* members can reduce NO_3^- to NO_2^-. Although these taxa are minor within the anammox granules, electrification may reshape the substrate structure available to anammox. Notably, short-term electrification altered the community relative to the continuously unelectrified control: *Denitratisoma*, *Hyphomicrobium*, and *Comamonas* increased, whereas *Thauera* decreased — changes that affect how anammox accesses substrate (Tab. 3).

Tab. 3. Potential zones, dominant communities, and dominant nitrogen-transformation pathways

Potential (V)	Dominant communites	Dominant nitrogen-transformation pathway
0.105~0.185	*Proteobacteria*↑ + *Candidatus Brocadia* (stable) + *Bacteroideta*↑ + *Campylobacterota*↓↓	Anammox-dominated
0.225~0.265	*Nitrospirota*↑↑ + *Geobacter*↑ + *Shewanella*↑ + *Candidatus Brocadia*↓ + *Rhodopirellula*↑	Anammox-dominant with weak nitrification and denitrification
0.305~0.345	*Nitrosomonas*↑↑ + *Alicycliphilus*↑ + *Clostridium*↑ + *Candidatus Brocadia*↓↓	Anammox-limited; enhanced nitrification side reaction and denitrification
0.385~0.433	*Pseudomonas*↑↑↑ + *Comamonas*↑↑ + *Campylobacterota*↑ + *Denitratisoma*↑ + *Ignavibacterium*↓↓	Multi-pathway nitrogen conversion

The up and down arrows indicate the degree of increase or decrease in the relative abundance of strains

3.3 Nitrogen-transformation pathways under stepwise potentials

To further resolve the non-anammox routes over E=+0.225~+0.433 V, metaproteomics was performed on the raw sludge and long-term electrified controls. The detected nitrogen-cycling proteins comprised: nitrification (AmoA_B, AmoB_B, AmoC_B, Hao, NxrB), denitrification (NarGHI, NarH, NarY, NarZ, NirK, NirS, NorB, NosZ), DNRA (NrfC), assimilatory nitrate reduction (glnA, gs_K00266, gdh_K00261, gdh_K00262), and nitrate assimilation (NarB). The anammox pathway was inferred from *Candidatus Brocadia* abundance and activity data rather than direct protein detection (Tab. 4).

Tab. 4 NCyc-category protein profiles (log_{10} of LFQ intensity) across potentials

Type	CE	Raw sludge	0.225V	0.265V	0.305V	0.345V	0.385V	0.433V
Assimilatory Nitrate Reduction	6.50	0.00	6.27	6.53	6.53	6.53	6.35	6.66
Denitrification	7.98	8.07	8.04	8.04	8.05	8.02	8.07	8.09
Denitrification-Dissimilatory Nitrate Reduction	7.59	7.68	7.92	7.57	7.59	7.64	7.68	7.58
Dissimilatory Nitrate Reduction	6.55	6.76	6.81	6.73	6.84	6.71	6.86	6.91
Nitrification	9.33	9.15	8.96	9.23	9.20	9.12	9.04	9.15
Organic Degradation Synthesis	8.84	9.20	9.38	9.07	8.96	9.10	9.30	9.16

Log_{10}(NCycDB type)

The denitrification proteins displayed a constitutive expression with weak potential dependence (Fig. 6). NarGHI (NO_3^-→NO_2^-) was constitutively expressed at moderate abundance ($1.88 \times 10^7 – 2.83 \times 10^7$) across all six potentials without significant potential dependence ($p > 0.05$), indicating that the biofilm system constitutively sustains nitrate-to-nitrite reduction. NirS (NO_2^-→NO) fluctuated mildly with potential ($2.73 \times 10^7 – 3.76 \times 10^7$) with a slight elevation at E=+0.385 V, suggesting that higher potentials modestly promote the NO_2^-→NO flux, consistent with increased electron availability at the cathode surface. NorB was detected at lower abundances (10^6–10^7), completing the full denitrification chain from NO_3^- to N_2.

The nitrification proteins displayed striking mid-potential hyperactivation. AmoA_B/AmoC_B, Hao, and NxrB collectively peaked at E=+0.265 V, with AmoB_B (category summation) reaching 1.18×10^9 — the highest single-protein abundance among all detected nitrogen-cycling enzymes. This peak coincided precisely with the maximum NO_3^- accumulation anomaly at E=+0.265 V, the rapid rise of AOB from 0.84% (E=+0.105 V) to 4.33% (E=+0.265 V), and the onset of NH_4^+-removal decline. This constituted evidence

for a nitrification side-reaction window centered at E=+0.265 ± 0.04 V. These proteins provided biological evidence for the nitrification activity.

The DNRA pathway was evidenced by NrfC. NrfC was detected in all potential samples, from a minimum of 5.10×10^6 at E=+0.345 V to a maximum of 8.08×10^6 at E=+0.433 V (a 58% increase). This potential-dependent upregulation suggested that DNRA was not merely a background pathway but was electrochemically stimulated at higher potentials, where excess electron flux favored complete reduction of NO_2^- to NH_4^+ over partial reduction to NO. If a fraction of NO_2^- was continuously recycled to NH_4^+ via DNRA, this created an internal ammonium recycling loop: NH_4^+ consumed by anammox → NO_2^- produced via partial nitrification → NH_4^+ regenerated by DNRA. This loop may explain the persistent discrepancy between measured NO_3^- accumulation and the theoretical anammox prediction over a wide potential range, and may sustain residual nitrogen removal where direct anammox activity is suppressed. Recent investigations have independently confirmed DNRA's underappreciated role in anammox-dominated systems, showing DNRA contributions of 15–22% to total nitrogen removal [42,50].

The anammox pathway was mainly determined by the dominant AnAOB genus (*Candidatus Brocadia*), whose abundance peaked (7.96%) at E=+0.305 V precisely when anammox activity was most suppressed (45.4% removal). This inversion definitively rules out simple cell lysis or washout as the inhibition mechanism. The organisms were present and may even be numerically dominant, yet their per-cell metabolic activity was severely compromised.

Three non-lethal mechanisms were proposed by which high cathodic potential (E >

+0.305 V) impaired anammox. (1) Enzyme-level inactivation. Both HZS and HDH contain iron–sulfur clusters that are exquisitely sensitive to redox poise. Sustained cathodic polarization shifted intracellular redox potential and may damage these metalloenzymes without immediate cell death. Research reported similar threshold behavior where AnAOB enzyme specific activity declined sharply above critical redox values while cell counts remained constant [32]. (2) Energy diversion. Under high-potential, excess electrons may be diverted to competing pathways such as DNRA or nitrogen side reactions, thereby depriving HZS and HDH of the reducing equivalents required for hydrazine synthesis. Shaw et al. [24] demonstrated that EET-dependent anammox required precise tuning of extracellular redox potential, deviations beyond the optimal window uncouple electron uptake from catabolism. (3) Regulation via key metabolic enzymes in response to environmental perturbation. Prior work [50] indicated that AnAOB responded to perturbation through phosphorylation of key metabolic enzymes. Moreover, the recovery experiment further supported that short-term high-potential inhibition of anammox was metabolic rather than structural.

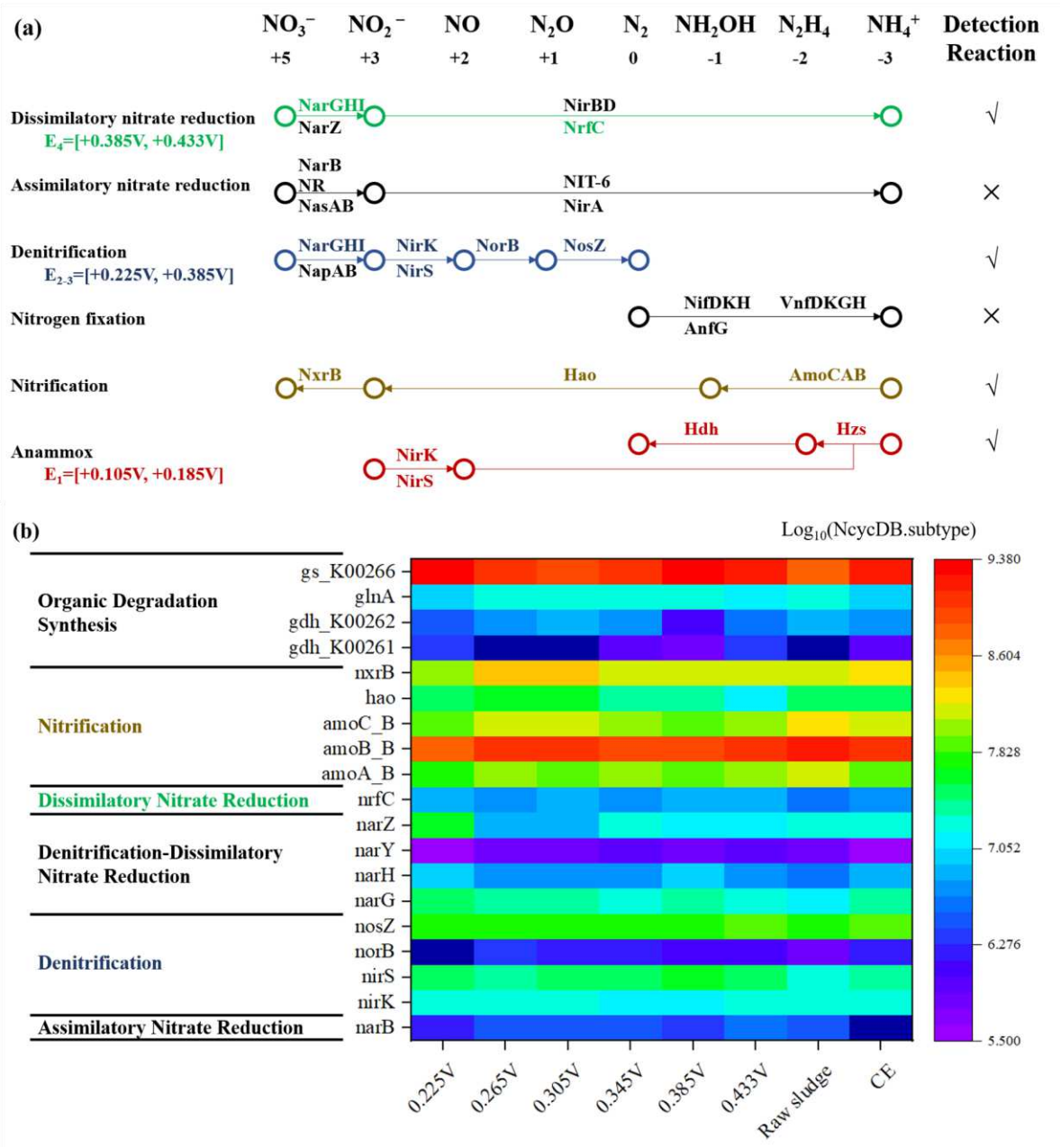


Fig. 6 Nitrogen transformation pathways and protein heatmap of each stepwise potential

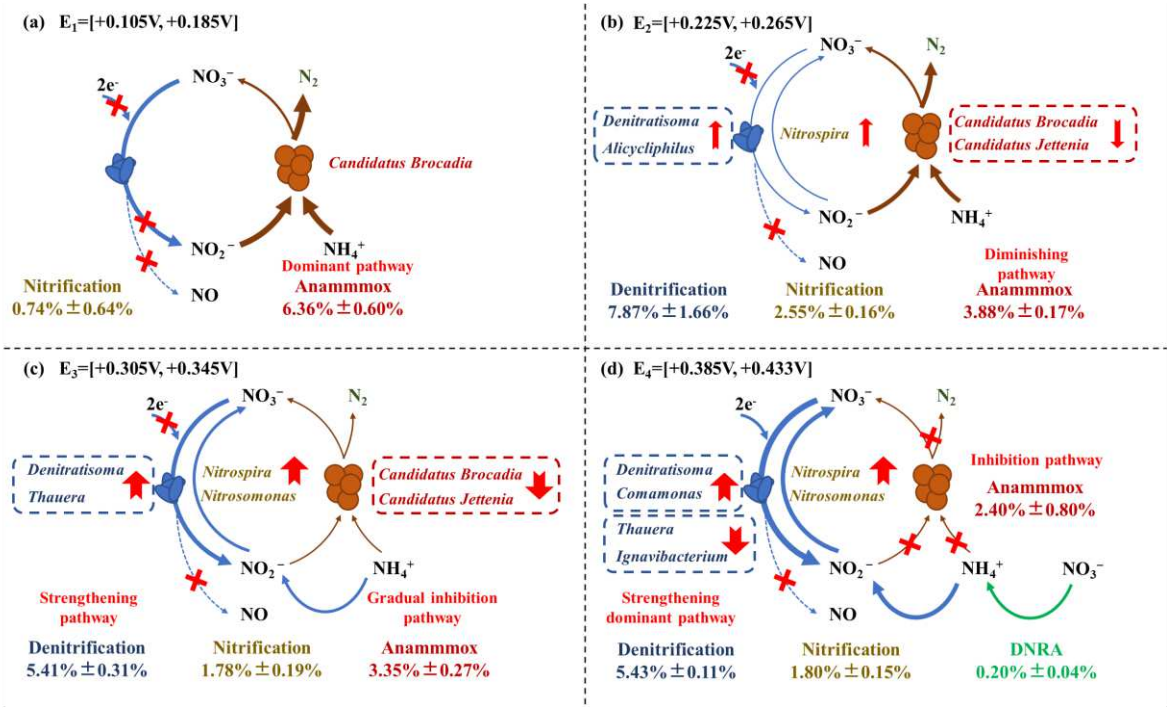


Fig. 7 Main nitrogen reaction pathways in different potential intervals

(a) The anammox-dominated window; (b) the anammox-dominant window with weak nitrification and denitrification; (c) anammox-limited, with enhanced nitrification side reactions and denitrification; (d) multi-pathway nitrogen conversion. The data show the proportions of nitrogen conversion via each pathway

Fig. 7a and 7d delineated the two edges of this double-edged sword most clearly. Moreover, at the highest potentials anammox was suppressed and declining and did not meaningfully participate in nitrogen conversion. First, DNRA was enhanced and created an internal NO_2^- cycle. Although the route was not anammox, NH_4^+ and NO_2^- declined together. Second, the electrochemical route strengthened NO_3^-→NO_2^- reduction. Third, *Comamonas* and other facultative bacteria can build electron-transfer paths via cytochrome c and other proteins to acquire electrons for nitrogen transformation through abiotic or heterotrophic pathways. This indicated that E=+0.105~0.185 V should be the primary operating, E=+0.225~0.345 V should be avoided or minimized in continuous operation. Finally, although E=+0.385~0.433 V offered DNRA-assisted nitrogen recycling that partially compensated the suppressed anammox conversion, it still inhibited system-level anammox

nitrogen removal.

3.4 Advantages and disadvantages of two-stage stepwise-potential-assisted anammox denitrification

A two-stage stepwise-potential-assisted anammox denitrification strategy (SPAD) was proposed to replace constant-potential operation with periodic stepwise operation, invoking a low-potential stage and a high-potential stage within each cycle. Stage I (anammox-enhancement stage). The applied potential was E=+0.145 V for 90 min to maximize the anammox rate to extensively consume NH_4^+ and NO_2^- at low current density. Stage II (non-anammox stage). The applied potential was E=+0.385 V for 30 min to reduce NO_3^- to NO_2^- electrochemically and to stimulate heterotrophic denitrification to polish residual nitrogen. DNRA would recycle part of the NO_2^- to NH_4^+ for the next cycle.

Relative to constant-potential operation, SPAD can avoid cumulative AnAOB damage from prolonged high-potential exposure, can exploit the multi-pathway capacity of the V-shaped rebound to activate compensatory pathways when anammox is most vulnerable, and can achieve TN removal exceeding the single-potential maximum through complementarity in principle. However, SPAD has limitations and risks. Frequent potential switching may impose biofilm shedding due to the change in the microenvironment. Stage II also requires N_2O emission monitoring and control. Moreover, the parameters (E_1, E_2, T_1, T_2) must be individually optimized based on the feed water parameters, such as C/N, pH, NH_4^+ concentration, total nitrogen load and nitrogen composition.

4 Conclusions

This study investigated the acute response mechanism of anammox biocathodes to

stepwise potential perturbations. Stepwise potential acted as a double-edged sword for anammox. A potential of E=+0.145 V was identified as optimal for short-term nitrogen removal via anammox. When the potential increased beyond E=+0.185 V, the nitrogen removal rate gradually declined, reaching a minimum at E=+0.345 V. This indicated that higher potentials suppressed nitrogen removal efficiency. Electrochemical reduction of NO_3^- to NO_2^- was confirmed under high-potential conditions, suggesting that a non-anammox pathway compensated for impaired anammox-driven denitrification. The most pronounced microbial response occurred within the first 90 min. The cathodic community, particularly *Candidatus Brocadia*, exhibited non-monotonic dynamics. Denitrifiers and nitrifiers became significantly enriched at moderate to high potentials, shifting the community structure from anammox dominance toward a multi-symbiotic pathway involving denitrification, nitrification, and anammox. Changes in *Candidatus Brocadia* abundance, applied potential magnitude, and nitrogen removal rates suggested that high-potential inhibition primarily damaged intracellular enzyme activity rather than causing cell death. Moreover, the inhibition of anammox under high potential was found to be reversible. The SPAD strategy was proposed as a novel approach for the efficient regulation of electrochemically assisted PD/A systems. Further studies need to evaluate the long-term stability, N_2O emission control, and applicability to real low-C/N wastewaters.

Credit author statement

L.Q. and W.X. wrote the main manuscript text, and L.Q. prepared the figures. L.Q. and Y.Y. conceived and designed the study. W.X. and J.L. developed the methodology. L.Q. and W.X. performed the validation, and W.X. conducted the experimental investigation. L.Q.,

S.S., L.W., Y.L., and L.Z. performed the formal analysis, with S.S. responsible for data curation. J.L., F.W., Y.L., and L.Z. provided the resources and materials. L.W., F.W., Y.Y., T.C., and S.L. supervised the work, and T.C. administered the project. L.Z. acquired the funding. All authors reviewed the manuscript.

Declaration of competing interest

The authors declare that they have no known competing financial interests or personal relationships that could have appeared to influence the work reported in this paper.

Acknowledgements

This work was supported by Jing-Jin-Ji Regional Integrated Environmental Improvement-National Science and Technology Major Project (2026ZD1217300), the National Natural Science Foundation of China (NSFC, Grant No. 52674244 and No. 52400059); the Natural Science Foundation of the Jiangsu Higher Education Institutions of China (No. 24KJB610017); and by the Major Project of Natural Science Foundation of Jiangsu Universities, China (24KJA610009).

References

[1] Kartal B, Kuenen J G, van Loosdrecht M C M. Sewage treatment with anammox[J]. Science, 2010, 328(5979): 702-703.

[2] Lackner S, Gilbert E M, Vlaeminck S E, et al. Full-scale partial nitritation/anammox experiences–an application survey[J]. Water Research, 2014, 55: 292-303.

[3] Du R, Cao S, Wang S, et al. Advanced nitrogen removal from wastewater by combining anammox with partial denitrification[J]. Bioresource Technology, 2015, 179: 497-504.

[4] Strous M, Heijnen J J, Kuenen J G, et al. The sequencing batch reactor as a powerful tool

553 for the study of slowly growing anaerobic ammonium-oxidizing microorganisms[J]. Applied
554 Microbiology and Biotechnology, 1998, 50(5): 589-596.
555 [5] Lotti T, Kleerebezem R, Lubello C, et al. Physiological and kinetic characterization of a
556 suspended cell anammox culture[J]. Water Research, 2014, 60: 1-14.
557 [6] Ma B, Wang S, Cao S, et al. Biological nitrogen removal from sewage via anammox:
558 Recent advances[J]. Bioresource Technology, 2016, 200: 981-990.
559 [7] Zhao Q, Ji J, Xie T, et al. Pilot-scale implementation of mainstream anammox for
560 municipal wastewater treatment against cold temperature[J]. Nature Communications, 2024,
561 15: 10314.
562 [8] Du R, Cao S, Li B, et al. Synergy of partial-denitrification and anammox in continuously
563 fed upflow sludge blanket reactor for simultaneous nitrate and ammonia removal at room
564 temperature[J]. Bioresource Technology, 2019, 274: 386-394.
565 [9] Ji J, Peng Y, Wang B, et al. Synergistic partial-denitrification, anammox, and in-situ
566 fermentation (SPDAF) process for advanced nitrogen removal from domestic and nitrate-
567 containing wastewater[J]. Environmental Science & Technology, 2020, 54(6): 3702-3713.
568 [10] Roots P, Wang Y, Rosenthal A F, et al. Comammox Nitrospira are the dominant ammonia
569 oxidizers in a mainstream low dissolved oxygen nitrification reactor[J]. Water Research,
570 2019, 157: 396-405.
571 [11] Zhao Y, Liu S, Jiang B, et al. Genome-centered metagenomics analysis reveals the
572 symbiotic organisms possessing ability to cross-feed with anammox bacteria in anammox
573 consortia[J]. Environmental Science & Technology, 2018, 52(19): 11285-11296.
574 [12] Du R, Cao S, Wang S, et al. Performance of partial denitrification (PD)-anammox

process in simultaneously treating nitrate and low C/N domestic wastewater at low temperature[J]. Bioresource Technology, 2016, 219: 420-429.

[13] Du R, Peng Y, Cao S, et al. Mechanisms and microbial structure of partial denitrification with high nitrite accumulation[J]. Applied Microbiology and Biotechnology, 2016, 100(4): 2011-2021.

[14] Cao S, Du R, Peng Y, et al. Novel two stage partial denitrification (PD)-anammox process for tertiary nitrogen removal from low carbon/nitrogen (C/N) municipal sewage[J]. Chemical Engineering Journal, 2019, 362: 107-115.

[15] Wang H, Ren Z J. A comprehensive review of microbial electrochemical systems as a platform technology[J]. Biotechnology Advances, 2013, 31(8): 1796-1807.

[16] Pous N, Puig S, Coma M, et al. Bioremediation of nitrate-polluted groundwater in a microbial fuel cell[J]. Journal of Chemical Technology & Biotechnology, 2013, 88(9): 1690-1696.

[17] Lefebvre O, Shen Y, Tan Z, et al. Full-loop operation and cathodic acidification of a microbial fuel cell operated on domestic wastewater[J]. Bioresource Technology, 2011, 102(10): 5841-5848.

[18] Ghafari S, Hasan M, Aroua M K. Bio-electrochemical removal of nitrate from water and wastewater—a review[J]. Bioresource Technology, 2008, 99(10): 3965-3974.

[19] Wang K, Zhang S. Extracellular electron transfer modes and rate-limiting steps in denitrifying biocathodes[J]. Environmental Science and Pollution Research, 2019, 26(16): 16378-16387.

[20] Ceballos-Escalera A, Pous N, Korth B, et al. Ex-situ electrochemical characterisation of

597 fixed-bed denitrification biocathodes: A promising strategy to improve bioelectrochemical
598 denitrification[J]. Chemosphere, 2024, 347: 140699.
599 [21] Wu Y, Wan Y, Tian L, et al. Bioelectrochemical partial-denitrification coupled with
600 anammox for autotrophic nitrogen removal[J]. Chemical Engineering Journal, 2022, 434:
601 134667.
602 [22] Zhang Z, Hou L, Liu W, et al. Start-up of coupled partial denitrification-anammox (PD/A)
603 process with external electric field for continuous wastewater treatment containing
604 ammonium and nitrate[J]. Journal of Environmental Chemical Engineering, 2025, 13(6):
605 119592.
606 [23] Dong X, Liu H, Long S, et al. Weak electrical stimulation on biological denitrification:
607 Insights from the denitrification enzymes[J]. Science of the Total Environment, 2022, 806:
608 150926.
609 [24] Shaw D R, Ali M, Katuri K P, et al. Extracellular electron transfer-dependent anaerobic
610 oxidation of ammonium by anammox bacteria[J]. Nature Communications, 2020, 11: 2058.
611 [25] Xia Y-G, Zhou J-H, Yang X-L, et al. Anodic potential and conductive carrier
612 synergistically drive nitrite-free extracellular electron transfer-dependent anaerobic
613 ammonium oxidation (Anammox) in mixed microbial communities[J]. Bioresource
614 Technology, 2026, 446: 134180.
615 [26] Qiao L, Yuan Y, Mei C, et al. Reinforced nitrite supplement by cathode nitrate reduction
616 with a bio-electrochemical system coupled anammox reactor[J]. Environmental Research,
617 2022, 204: 112051.
618 [27] Liu Y, Zhu Y, Wu D, et al. Effect of free nitrous acid on nitritation process: Microbial

619 community, inhibitory kinetics, and functional biomarker[J]. Bioresource Technology, 2023,
620 371: 128595.
621 [28] Yin X, Qiao S, Zhou J, et al. Using three-bio-electrode reactor to enhance the activity of
622 anammox biomass[J]. Bioresource Technology, 2015, 196: 376-382.
623 [29] Cai T, Lu X, Zhang Z, et al. Spatial distribution and nitrogen metabolism behaviors of
624 anammox biofilms in bioelectrochemical system regulated by continuous/intermittent weak
625 electrical stimulation[J]. Journal of Cleaner Production, 2022, 336: 130486.
626 [30] Hu Z, Li J, Zhang Y, et al. Exerting applied voltage promotes microbial activity of
627 marine anammox bacteria for nitrogen removal in saline wastewater treatment[J]. Water
628 Research, 2022, 215: 118285.
629 [31] Pous N, Koch C, Colprim J, et al. Extracellular electron transfer of biocathodes:
630 Revealing the potentials for nitrate and nitrite reduction of denitrifying microbiomes
631 dominated by Thiobacillus sp[J]. Electrochemistry Communications, 2014, 49: 93-97.
632 [32] Zhao Y, Duan H, Erler D, et al. Decoupling the simultaneous effects of NO_2^-, pH and
633 free nitrous acid on N_2O and NO production from enriched nitrifying activated sludge[J].
634 Water Research, 2023, 245: 120609.
635 [33] Kuypers M M M, Marchant H K, Kartal B. The microbial nitrogen-cycling network[J].
636 Nature Reviews Microbiology, 2018, 16(4): 263-280.
637 [34] Liu H, Qin S, Li A, et al. Bioelectrochemical systems for enhanced nitrogen removal
638 with minimal greenhouse gas emission from carbon-deficient wastewater: A review[J].
639 Science of the Total Environment, 2023, 859(Part 1): 160183.
640 [35] Han Z, Fang R, Wang X, et al. Nitrite acts as the key "switch" governing the free nitrous

641 acid pretreatment in anaerobic digestion: A comprehensive mechanism of abiotic,
642 bioinformatics and bioenergetics effects[J]. Chemical Engineering Journal, 2024, 480:
643 148051.
644 [36] Tang M, Guo Z, Xu X, et al. Performance and microbial mechanism of eletrotrophic
645 bio-cathode denitrification under low temperature[J]. Journal of Environmental Management,
646 2023, 328: 116960.
647 [37] Priks H, Zekker I, Manuell Nava A I, et al. Enhanced anammox-mediated nitrogen
648 removal in bioelectrochemical systems at prolonged negative electrode potentials[J].
649 Environmental Science and Pollution Research, 2024, 31: 63312-63324.
650 [38] Tang X, Yao Q, Jiang X, et al. Response of ammonium transformation in bioanodes to
651 potential regulation: Performance, electromicrobiome and implications[J]. Bioresource
652 Technology, 2025, 415: 131731.
653 [39] Jiang Z, He Y, Zeng M, et al. Revealing critical functional enzymes in anammox nitrogen
654 removal and rate-limiting step in catalytic pathways: Insight into metaproteomics and density
655 functional theory[J]. Bioresource Technology, 2024, 406: 131090.
656 [40] Wang Z, Li Y, Wu L, et al. Ferroheme/Ferriheme Directly Involved in the Synthesis and
657 Decomposition of Hydrazine as an Electron Carrier during Anammox[J]. Environmental
658 Science & Technology, 2024, 58(20): 10140-10148.
659 [41] Zheng R, et al. Siderophore-Mediated Cooperation in Anammox Consortia[J].
660 Environmental Science & Technology, 2025, 59: 4003-4013.
661 [42] Wang C, Qiao S. Electron transfer mechanism of intracellular carbon-dependent DNRA
662 inside anammox bacteria[J]. Water Research, 2023, 244: 120443.

[43] Dong T, Zhang L, Hao S, et al. Interspecies cooperation-driven photogenerated electron transfer processes and efficient multi-pathway nitrogen removal in the g-C_3N_4-anammox consortia biohybrid system[J]. Water Research, 2024, 255: 121532.

[44] Guo M, Lu X, Qiao S. Nitrate removal by anammox bacteria utilizing photoexcited electrons via inward extracellular electron transfer channel[J]. Water Research, 2024, 250: 121059.

[45] Lawson C E, Wu S, Bhattacharjee A S, et al. Metabolic network analysis reveals microbial community interactions in anammox granules[J]. Nature Communications, 2017, 8: 15416.

[46] Tu Q, Lin L, Cheng L, et al. NCycDB: a curated integrative database for fast and accurate metagenomic profiling of nitrogen cycling genes[J]. Bioinformatics, 2019, 35(6): 1040-1048.

[47] Qiao L , Xu W , Mao S ,et al.Study on the expanded culture and kinetics of anammox bacteria in the upper flow packed bed.[J]. The Science of the total environment, 2019, 650(Pt 1):1173-1181.

[48] Du R, Cao S, Li B, et al. Performance and microbial community analysis of a novel DEAMOX based on partial-denitrification and anammox treating ammonia and nitrate wastewaters[J]. Water Research, 2017, 108: 46-56.

[49] Yu L, Yuan Y, Chen S, et al. Direct uptake of electrode electrons for autotrophic denitrification by Thiobacillus denitrificans[J]. Electrochemistry Communications, 2015, 60: 126-130.

[50] Wang D, Zhang X, Zhang X, et al. Metabolic enhancement of AnAOB via enzyme and cofactor regulation for nitrogen removal in wastewater: a critical review[J]. Water Research,

685 2026: 126035.

Supplementary Files

This is a list of supplementary files associated with this preprint. Click to download.

- supplementarymaterials.rar